

# GAMMA-RAY BURSTS AND X-RAY MELTING OF MATERIAL AS A POTENTIAL SOURCE OF CHONDRULES AND PLANETS.

Paul Duggan<sup>1</sup>, Brian McBreen<sup>\*1</sup>, Alun J. Carr<sup>2</sup>, Sheila McBreen<sup>1</sup>, Elaine Winston<sup>1</sup>, Lorraine Hanlon<sup>1</sup>, and Leo Metcalfe<sup>3</sup>

<sup>1</sup>Department of Experimental Physics, University College Dublin, Ireland.

<sup>2</sup>Department of Mechanical Engineering, University College Dublin, Ireland.

<sup>3</sup> XMM-Newton Science Operations Centre, European Space Agency, Villafranca del Castillo, PO Box 50727, 28080 Madrid, Spain.

## ABSTRACT

The intense radiation from a gamma-ray burst (GRB) is shown to be capable of melting stony material at distances up to 300 light years which subsequently cool to form chondrules. These conditions were created in the laboratory for the first time when millimeter sized pellets were placed in a vacuum chamber in the white synchrotron beam at the European Synchrotron Radiation Facility (ESRF). The pellets were rapidly heated in the X-ray and gamma-ray furnace to above 1400 °C melted and cooled. This process heats from the inside unlike normal furnaces. The melted spherical samples were examined with a range of techniques and found to have microstructural properties similar to the chondrules that come from meteorites. This experiment demonstrates that GRBs can melt precursor material to form chondrules that may subsequently influence the formation of planets. This work extends the field of laboratory astrophysics to include high power synchrotron sources.

Key words: Gamma ray bursts, chondrules, planetary formation, laboratory astrophysics, X-ray melting, Synchrotron radiation.

## 1. INTRODUCTION

Chondrules are millimetre-sized, stony spherules (Fig. 1) that constitute the major component of most chondritic meteorites that originate in the region between Mars and Jupiter and which fall to the Earth. They appear to have crystallised rapidly from molten or partially molten drops and were described (Sorby 1877) as “molten drops in a fiery rain”. The properties of the chondrules and chondrites have been exquisitely deduced from an extensive series of experiments (Wasson & Rubin 2003; Hewins & Fox 2004) and two conferences have been devoted completely to chondrules (King 1983; Hewins et al. 1996). The mineralogy of chondrules

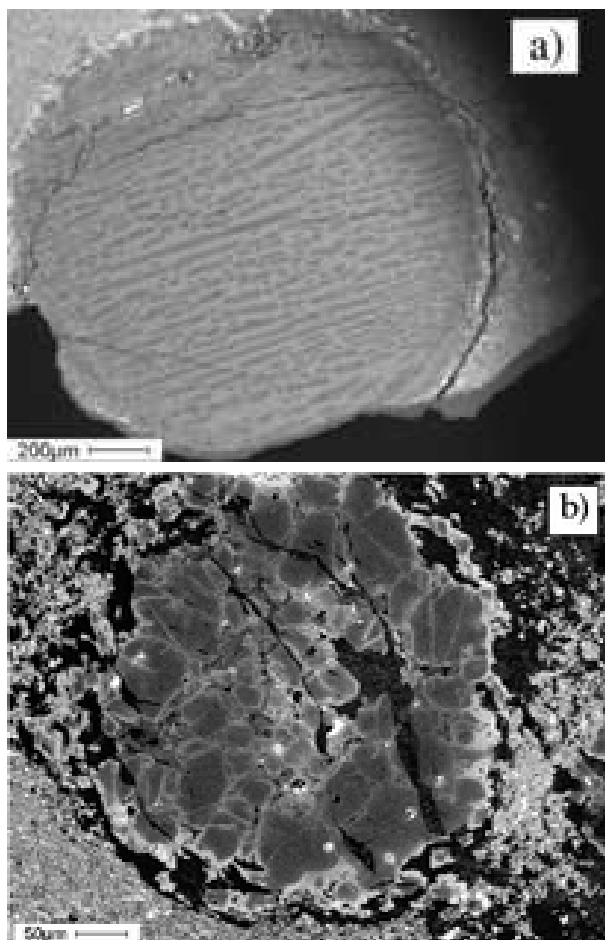
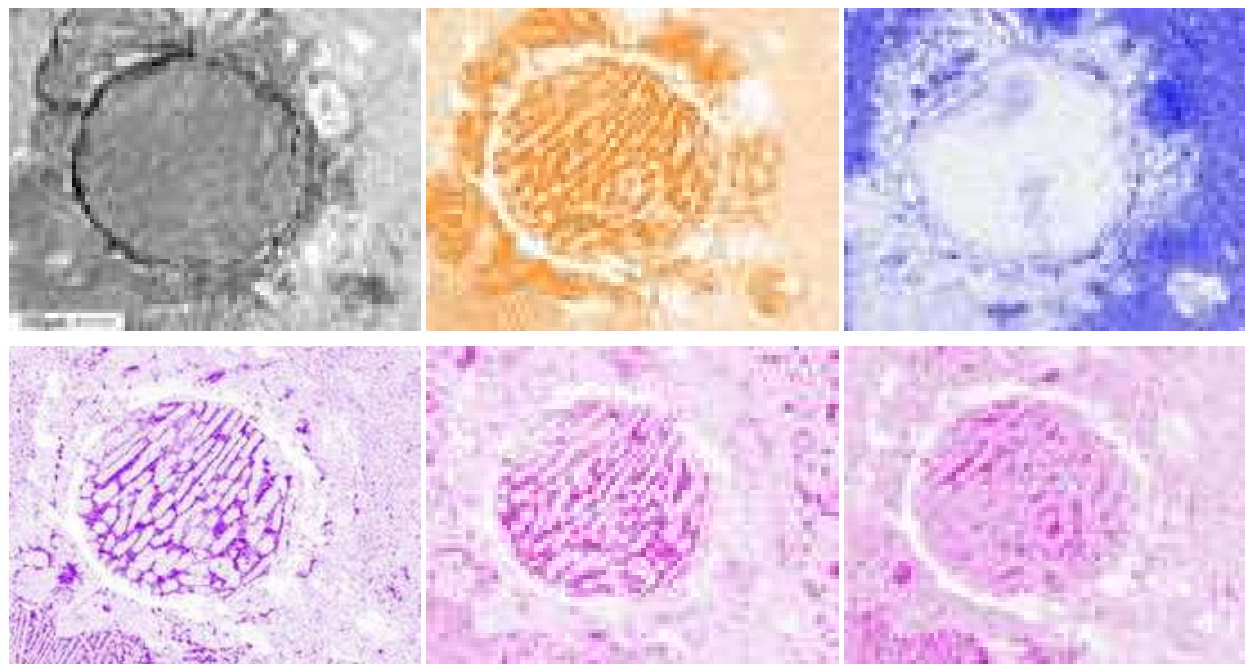


Figure 1. Backscattered electron microscope images of two chondrules from the Allende meteorite. Phases with higher atomic number are brighter in color. The dark grey grains are elongated olivine crystals in (a) and porphyritic crystals in (b) where the brighter regions are the interstitial glassy material. The diameters of the chondrules are about 1 mm and 0.6 mm and are surrounded by matrix material in the meteorite.

\*Correspondence to [brian.mcbreen@ucd.ie](mailto:brian.mcbreen@ucd.ie)



*Figure 2. Backscattered electron microscope image and X-ray maps of a chondrule from the Allende meteorite. In the case of the X-ray elemental maps, regions with greater proportions of an element have more intense colour. These images are created by analysing an X-ray window around the  $K_{\alpha}$  spectral line for each element during the raster scan by the electron beam. Top row from left: (a) backscattered electron image, (b) Mg X-ray map and (c) Fe X-ray map. Bottom row from left: (d) Al X-ray map, (e) Ca X-ray map and (f) Na X-ray map. The Mg is preferentially located in the olivine crystals (b) and the glassy material between the olivine crystals is enriched with Al and Ca (d and e). There is more iron in the matrix material surrounding the chondrule (c) as shown by the dark region.*

is dominated by olivine ( $(\text{Mg,Fe})_2\text{SiO}_4$ ) and pyroxene ( $(\text{Mg,Fe})\text{SiO}_3$ ) and there is a wide range of compositions for all elements. A compositional map of a chondrule is shown in Fig. 2. The magnesium is preferentially found in the dark olivine crystals (Fig. 2(b)) while the aluminium and calcium are located in the glassy material between the crystals (Fig. 2(d) and Fig. 2(e)). The diversity of chondrules is consistent with the melting of heterogeneous precursor solids or dust balls. The age of chondrules indicate they formed very early in the solar system. The calcium-, aluminium-rich inclusions (CAIs) are refractory inclusions in carbonaceous and ordinary chondrites that predate the chondrules by several million years and are the oldest known solid materials produced in the nebula (Swindle et al. 1996). The first  $10^7$  years in the complicated development of the solar system has been comprehensively covered in an attempt to understand the CAI to chondrule time interval of several million years (Cameron 1995).

The presence of volatile elements in the chondrules (Fig. 2(f)) indicate that the high temperature melting period lasted for a matter of seconds to minutes. Experiments based on chemical and textural compositions of chondrules suggest cooling rates that were much slower than radiative cooling of isolated chondrules and imply they were made in some large quantity in relatively opaque nebular domains (Yu & Hewins 1998; Brearley & Jones 1998). Volatile elements such as alkalis and sulphur occur in chondrule interiors as primary constituents and indicate that some chondrule precursor materials must have reacted with cool nebula gases at am-

bient temperatures less than 650 K.

The identification of the heat source responsible for chondrule formation is important for the understanding of the formation of planets because of the large amount of chondrules present in chondrite meteorites. The heat source remains uncertain and a critical summary of the heating mechanisms was given by Rubin (2000). These methods include bipolar outflows (Sekiya 1998; Lee et al. 1998) and shock wave heating of the precursor materials (Wood 1988; Miura & Nakamoto 2004; Ciesla & Hood 2002). Almost all proposed heat sources (Rubin 2000; Boss 1996; Jones et al. 2000) are local to the solar nebula, one exception being the proposal (McBreen & Hanlon 1999; Duggan et al. 2001) that the chondrules were flash heated to melting point by a nearby GRB when the iron all through the precursor material efficiently absorbed X-rays and low energy  $\gamma$ -rays. The distance to the source was about 300 light years (or 100 pc) for a GRB output of  $10^{53}$  erg and was estimated using the minimum value of  $2 \times 10^{10}$  erg  $\text{g}^{-1}$  required to heat and melt the precursor grains (Grossman et al. 1988; Wasson 1993). The role of nearby supernovae that preceded the formation of the solar system have been considered (Cameron 1995) along with the serious consequences for life on Earth of nearby supernovae (Ruderman 1974; Clark et al. 1977) and GRBs (Thorsett 1995; Scalo & Wheeler 2002). The consequences of a nearby GRB on the early solar nebula have not been considered elsewhere.

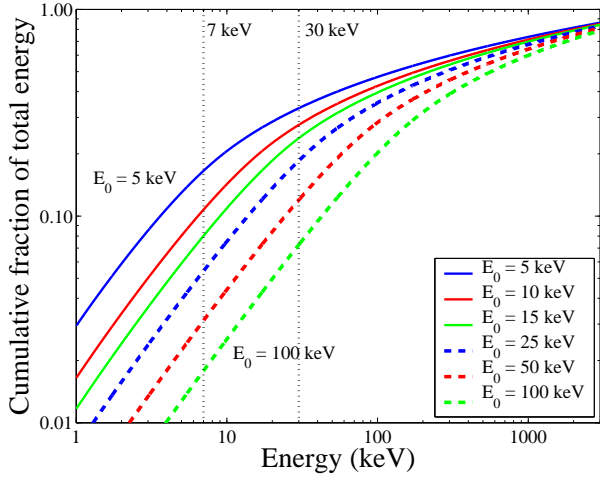


Figure 3. The cumulative fraction of GRB energy as a function of photon energy for assumed spectral parameters  $\alpha = -1$ ,  $\beta = -2$ ,  $E_0 = 5, 10, 15, 20, 25, 50$  and  $100$  keV and redshift of  $0.8$ .

## 2. GRBS AS A HEAT SOURCE

Since their discovery thirty years ago the properties of GRBs have been determined by an outstanding series of experiments that were deployed on more than twenty spacecraft at distances up to several astronomical units (AU) from the Earth and during one period 11 spacecraft were used to study the same GRBs. The properties of GRBs have been reviewed (Fishman & Meegan 1995; Piran 1999; Hurley et al. 2002; Zhang & Meszaros 2003) and are the subject of intense research. GRBs are extragalactic in origin and release colossal amounts of energy,  $10^{52}$  to  $4 \times 10^{54}$  erg assuming isotropic emission, for the GRBs with known redshift. The index of the X-ray afterglow is in the range  $t^{-1.1}$  to  $t^{-1.5}$  (Costa et al. 1997; Piro 2004; Nicastro et al. 1998). Simultaneous optical emission was detected from the spectacular GRB 990123 at the level of about  $10^{-5}$  of the energy in  $\gamma$ -rays (Akerlof et al. 1999), but this emission is too weak to influence chondrule formation.

The photon spectra of GRBs are well described by a power-law with a low energy slope  $\alpha$ , a break energy  $E_0$  and a high energy power law with slope  $\beta$ . The functional form is given by (Band et al. 1993):

$$N(E) = AE^\alpha e^{-E/E_0} \text{ and } N(E) = BE^\beta, \alpha > \beta.$$

The value of  $E_0$  ranges from 2 keV to over 1 MeV and the indices  $\alpha$  and  $\beta$  are typically  $-1$  and  $-2$  respectively. It is interesting to note that the temporal properties of the long and short GRBs are more complex than their spectral properties and are well described by a lognormal distribution (McBreen et al. 2001; Quilligan et al. 2002; McBreen et al. 2002a).

The spectral energy distributions of a sample of GRBs have been extrapolated and integrated from 0.1 keV to 10 MeV using a sample of values for  $E_0$  compatible with BATSE (Band et al. 1993) and Ginga results (Strohmayr et al. 1998). The cumulative fraction of the

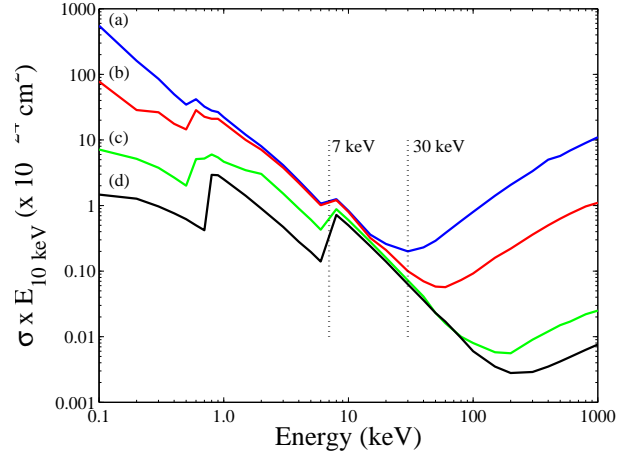


Figure 4. The combined photoelectric and Compton cross-sections relative to H as a function of energy and scaled by  $E/10$  keV for clarity of presentation. (a) The elements H to Fe that are at least as abundant as Fe (H, He, C, N, O, Ne, Mg, Si, Fe) (b) the same elements as in (a) with solar abundance of H and He reduced by 10% (c) The precursor dust combination  $Mg_{1.1}Fe_{0.9}SiO_4$  and (d) the element Fe.

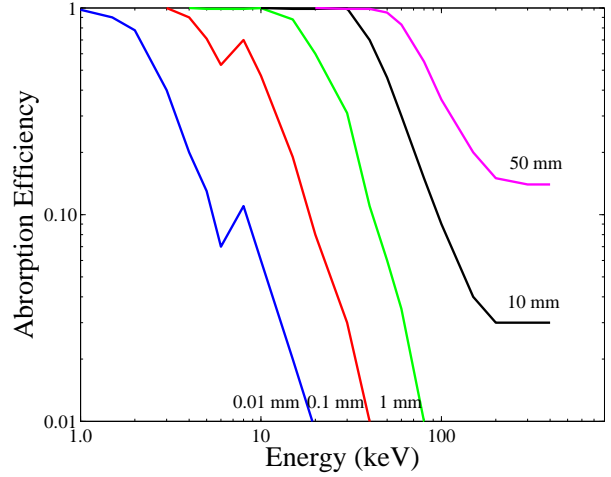


Figure 5. The absorption efficiency of different thickness of  $Fe_{0.9}Mg_{1.1}SiO_4$  as a function of energy: (a) 0.01 mm, (b) 0.1 mm, (c) 1 mm, (d) 10 mm, (e) 50 mm.

total energy in GRBs is given in Fig. 3 where a redshift correction of  $z = 0.8$  has been applied to all the spectra.

## 3. ATTENUATION OF X-RAYS AND $\gamma$ -RAYS

The absorption of the GRB energy by the gas and dust in the nebula would have occurred through the processes of photoelectric absorption and Compton scattering. The combined cross-sections due to these processes for the elements from H to Fe are plotted in Fig. 4. Solar abundance values were adopted for the nebula (Anders & Grevesse 1989) and the photoelectric and Compton cross-sections for the elements have been used (Veigele 1973). The photoelectric effect absorbs the pho-

Table 1. Elemental oxide compositions of three types of precursor material in weight percentages and the calculated liquidus temperatures. The compositions are the same as listed (Yu & Hewins 1998) except that the small amounts of  $K_2O$  ( $< 0.11\%$ ) were not included and magnetite ( $Fe_3O_4$ ) was used in place of  $FeO$ .

	Type IA	Type IAB	Type II
$SiO_2$	45.4	47.2	49.2
$TiO_2$	0.1	0.1	0.1
$Al_2O_3$	4.9	9.7	4.1
$Fe_3O_4$	8.3	6.6	21.3
$MnO$	0.1	0.1	0.1
$MgO$	37.4	30.7	22.7
$CaO$	2.5	3.5	0.2
$Na_2O$	1.3	2.1	2.3
Liquidus Temperature	1,692 °C	1,577 °C	1,509 °C

ton completely but in Compton scattering only a fraction of the energy is removed per scattering and this fraction varies from 0.14 at 100 keV to 0.45 at 1 MeV. The product of the Compton cross-section by the fraction of the energy absorbed in the first scattering was used for the Compton cross-section and many scatterings may occur before the degraded photon is finally absorbed by the photoelectric effect. Decreasing the abundance of H and He by a factor of 10 relative to the solar value significantly reduces the cross-section below 1 keV and above 20 keV (Fig. 4(b)). The Fe cross-section (Fig. 4(d)) is dominant between the K absorption edge at 7.1 keV and 30 keV but the upper bound of 30 keV extends to above 50 keV for low abundance of H and He. Fe makes the major contribution to the absorption by the dust and is the key to chondrule formation.

A composition consisting of solar abundance of oxides of Fe, Si and Mg or  $Mg_{1.1}Fe_{0.9}SiO_4$  was assumed for the precursor grains and the product of the cross-section of this combination by abundance relative to H is plotted in Fig. 4(c). The X-ray and  $\gamma$ -ray absorption efficiencies of different thicknesses of precursor grains, assuming a density of one, are given in Fig. 5 and grains in the range 0.01 mm to 50 mm are very efficient absorbers in the region where dust dominates the absorption (Fig. 4). This range agrees quite well with the measured Weibull and lognormal distributions of chondrule sizes (Martin & Hughes 1980; Rubin & Keil 1984). The deficiency of small grains is caused by low absorption efficiency and substantial radiation losses from grains with large surface to volume ratios. The thickness of the dust layer converted to chondrules depends on the GRB spectrum which must have significant emission below 30 keV where dust absorption dominates (Fig. 4) and also on the mixture and distribution of gas and dust in the nebula. For a GRB with  $10^{53}$  erg and an assumed spectrum  $\alpha = -1$ ,  $\beta = -2$  and  $E_0 = 15$  keV (Fig. 3), the fraction of GRB energy photoelectrically absorbed by the dust is 20%, increasing to 27% for a factor 10 reduction in H and He. In the simplified case of solar abundance and a uniform mix of gas and dust, the thickness of the chondrule layer created is  $0.18 \text{ g cm}^{-2}$  corresponding to one optical depth for 30 keV X-rays. The layer

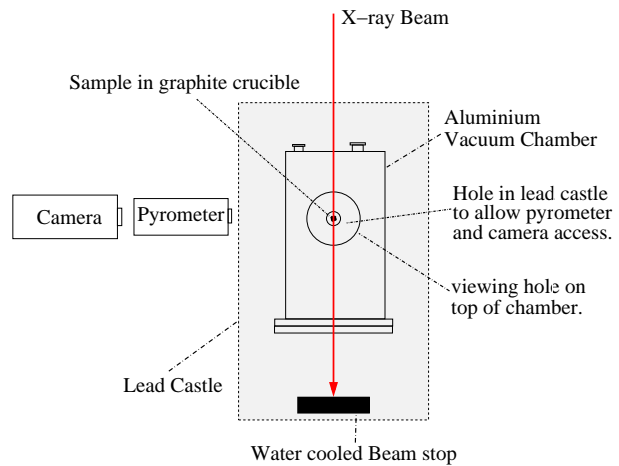


Figure 6. Schematic diagram of experimental setup at the ESRF. The lead castle shield encasing the experiment is shown by the grey box.

thickness increases to about  $0.8 \text{ g cm}^{-2}$  and  $2.0 \text{ g cm}^{-2}$  for optical depths to 40 keV and 55 keV X-rays with H and He abundances reduced by factors of 3 and 10 respectively. The thickness of the chondrule layer is therefore controlled by the degree of gas depletion from the nebula. The minimum GRB fluence required to produce chondrule layers of  $0.18$ ,  $0.8$  and  $2.0 \text{ g cm}^{-2}$  is  $1.8 \times 10^{10}$ ,  $7.0 \times 10^{10}$  and  $1.5 \times 10^{11} \text{ erg cm}^{-2}$ , adopting 20%, 23% and 27% absorption by the chondrule precursors and  $2 \times 10^{10} \text{ erg g}^{-1}$  for heating and melting. A fluence of  $10^{11} \text{ erg cm}^{-2}$  implies a distance of about 100 pc to the source for an output of  $10^{53}$  erg radiated isotropically. The GRB would also form a layer of chondrules over a large area ( $10^3 - 10^4 \text{ pc}^2$ ) in a nearby molecular cloud provided large precursor grains had already formed (Weidenschilling & Ruzmaikina 1994). The process of chondrule amalgamation might be sufficient to trigger star formation over this region. In this case chondrule formation precedes cloud collapse and star formation. The existence of pre-solar grains in meteorites is well established (Zinner 1996) but there is no evidence for pre-solar chondrules.

The distance to the source could be up to 300 light years ( $\sim 100 \text{ pc}$ ) for a GRB with an isotropic output of  $10^{53}$  erg (Piran 1999; Mészáros 2002). This distance limit was obtained using the minimum value of  $2 \times 10^{10} \text{ erg g}^{-1}$  required to heat and melt the precursor grains (Wasson 1993) and is equivalent to an enormous energy deposition of  $10^{11} \text{ erg cm}^{-2}$ .

#### 4. EXPERIMENTAL METHOD

It is now possible to create the astrophysical conditions near a GRB source in the laboratory due to the development of powerful synchrotrons (Duggan et al. 2003). The ESRF has a 6 GeV, third-generation synchrotron capable of generating the required power. A wiggler device was inserted and used to create X-rays in the range 3 – 200 keV. The 24-pole wiggler has a characteristic energy of 29 keV at a minimum wiggler gap of 20.3 mm.

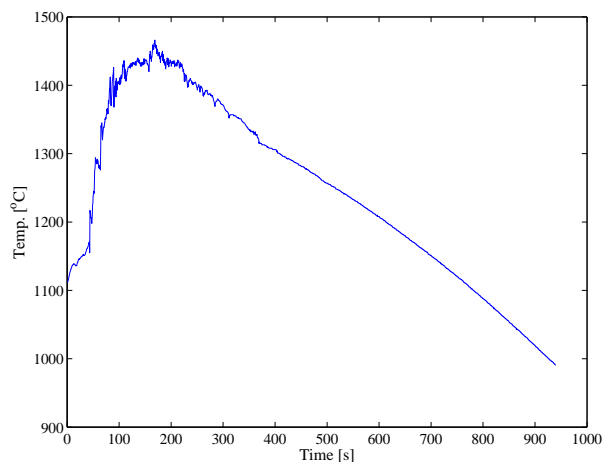


Figure 7. The temperature profile of a typical sample in the synchrotron experiment. The reason for the high initial temperature is that  $1000^{\circ}\text{C}$  is the minimum value read by the pyrometer. The temperature rose rapidly to above  $1000^{\circ}\text{C}$  when the beam shutter was opened.

Time was awarded on the ID11 white beam to test the prediction that large fluxes of X-rays and  $\gamma$ -rays could melt millimetre sized dust grains and hence extend the use of high power synchrotron sources to laboratory astrophysics (Remington et al. 1999). The composition of chondrules varies widely and a classification system based on the iron content is often used (McSween 1977; Yu & Hewins 1998). Type IAB chondrules have low iron content while type IA and type II have increasing amounts of iron. The pellets were made from a mixture of elemental oxides with weight percentages as given in Table 1 for the three precursors types.

The major effect of including more iron is to reduce the magnesium content and the liquidus temperature of the material. The oxides, without the volatile  $\text{Na}_2\text{O}$ , were mixed and heated to  $400^{\circ}\text{C}$  in an alumina crucible for 13 hours. The powders after heating had a mass loss of about 5%, due to moisture loss and reduction of the elemental oxides. After cooling,  $\text{Na}_2\text{O}$  was added to the mixture. The powder was pressed into cylindrical pellets of diameter 3 mm and height of 3 mm.

Each pellet was placed in a graphite crucible inside an evacuated container and inserted into the path of the white X-ray beam (Fig. 6). The size of the beam was  $2\text{ mm} \times 1.5\text{ mm}$ . The synchrotron beam entered the vacuum chamber through a Kapton window of thickness 0.05 mm. The pressure in the container was between  $10^{-2} - 10^{-3}\text{ mbar}$ , which is typical of planetary forming systems. In a few cases the residual air in the vacuum chamber was replaced with hydrogen. During the heating cycle the temperature of the pellet was measured using a Raytex MR1SCSF pyrometer with a range from  $1000^{\circ}\text{C}$  to  $3000^{\circ}\text{C}$ . The pyrometer was located outside the lead shielding and viewed the sample via a mirror through a glass window on the top of the vacuum container and at right angles to the X-ray beam. This window had to be replaced on several occasions during the experiment because of darkening caused by radiation damage. The sample was also monitored with a camera that viewed it

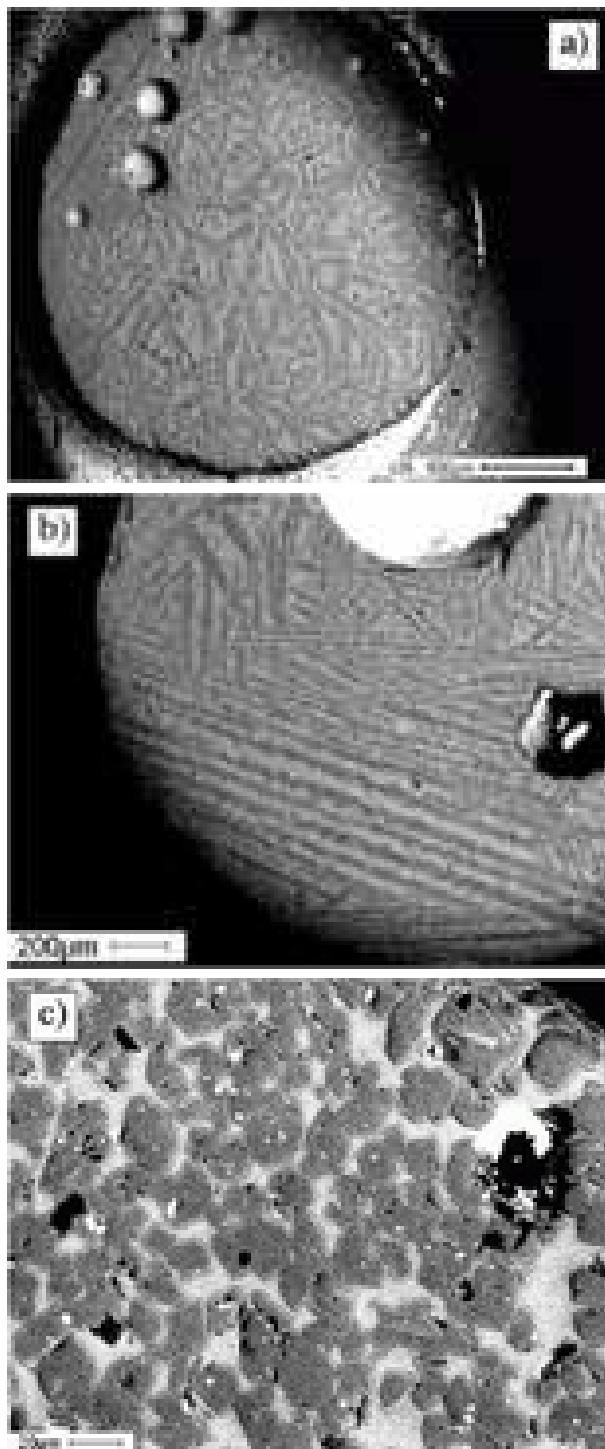


Figure 8. Backscattered electron microscope images of three melted samples from the synchrotron experiment. (a) cross-section of a complete sample with randomly orientated olivine crystals and type IA precursor composition. (b) section of a sample with barred olivine crystals and type II precursor composition (c) section of a sample with porphyritic crystals and type IAB precursor composition. The samples in (a) and (b) have cavities of size  $< 500\mu\text{m}$ . Cavities have been observed (Maharaj & Hewins 1994) in other experimentally produced samples and are caused by trapped gases and incomplete melting.



Figure 9. Electron microscope image and X-ray maps of a section of type IA X-ray heated sample. Top row from left: (a) secondary electron image with  $\times 1000$  magnification (the black bar in the bottom left hand corner measures  $10\ \mu\text{m}$ ), (b) Mg X-ray map and (c) Fe X-ray map. Bottom row from left: (d) Al X-ray map, (e) Ca X-ray map and (f) Na X-ray map. The partitioning of the elements is similar to that shown in the chondrule in Fig. 2. The Mg is concentrated in the olivine crystals and the Al and Ca are enhanced in the glassy material between the crystals.

through the pyrometer optics. The pellets were rapidly heated in the X-ray and  $\gamma$ -ray furnace to temperatures above  $1400^\circ\text{C}$  (Fig. 7). During the heating and melting process the pellets bubbled, moved about and sometimes ejected small drops of iron rich material. The melted samples were kept at the maximum temperature for a duration of 10 s to 300 s and cooled when the power in the beam was reduced by widening the gap between the magnets of the wiggler. The beam was removed when the temperature dropped below  $1000^\circ\text{C}$ . The samples cooled rapidly to yield 2–3 mm diameter black spherules.

A Huber model 642 Guinier X-ray powder diffractometer with monochromatic  $\text{Cu K}\alpha_1$  radiation was used for powder diffraction. Aluminium foil was placed between the sample and detector to reduce the fluorescent background from iron. The crystal phases were identified using the JCPDS Powder Diffraction File. Crystal structures were refined using Rietveld analysis in the range  $20^\circ < 2\theta < 100^\circ$  using Rietica (Hunter 1998; Hill & Howard 1987). For angular calibration and quantitative phase analysis a known mass of high-purity silicon (9% to 16% by mass depending on the sample) was added as an internal standard to the powdered sample. Refined structural variables included lattice parameters, atomic coordinates, metal site occupancies and isotropic temperature factor; nonstructural variables included scale factors, background correction and peak shape. Absorption effects were treated as though they were part of the overall isotropic temperature factor (Scott 1981).

## 5. RESULTS

A total of 24 samples were melted and cooled in the radiation beam. Backscattered electron microscope images of three samples are given in Fig. 8. One sample (Fig. 8(a)) has olivine crystals orientated in a random pattern whereas the sample in Fig. 8(b) has a barred olivine texture. The sample in Fig. 8(c) has porphyritic microstructure. A compositional X-ray map of a type IA sample is shown in Fig. 9 and has similar olivine crystalline structure and composition to the chondrule in Fig. 2.

There was a general tendency for the microstructure of the samples to reflect the liquidus temperature (Yu & Hewins 1998). Type IA samples have the highest liquidus temperature of  $1692^\circ\text{C}$  (Table 1). The type IA samples were predominantly porphyritic in texture with smaller crystals while IAB were about equal mixture of porphyritic and acicular olivine whereas acicular olivine predominated in type II. The type IA samples with highest liquidus temperature had more nuclei throughout the partial melt at the start of cooling on which the crystals could grow (Rubin 2000). The greater number of nucleation sites resulted in more crystals with smaller dimensions. Type II samples had the least number of nucleation sites resulting in fewer but larger crystals. The faster the cooling rate the more imperfect the crystals that formed. There is not a perfect match between the microstructure of chondrules (Fig. 1) and the samples produced in the synchrotron beam (Fig. 8). The final texture of samples depends on a range of factors (Rubin 2000; Connolly et al. 1998; Lofgren & Lanier 1990) such as the

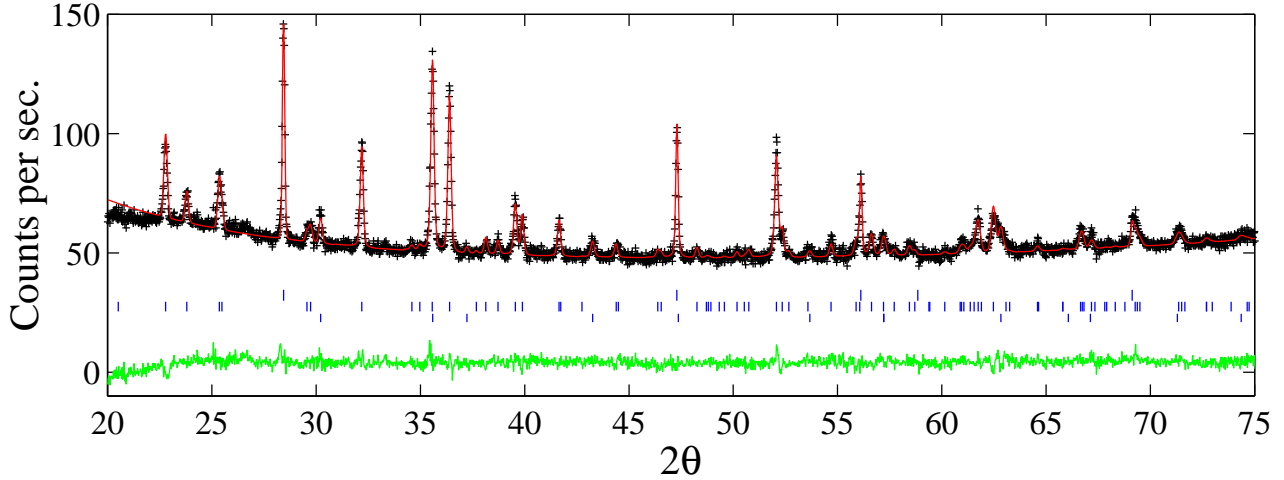


Figure 10. X-ray diffraction pattern of a type II sample. The data are plotted with crosses and the calculated profile is shown as a continuous line. The three sets of vertical bars in the middle of the figure are the calculated reflection positions for silicon used for calibration purposes (top), olivine (middle) and magnetite (bottom). The residuals between the data and the calculated profile are shown at the bottom of the figure indicating a very good match.

precursor composition, maximum temperature, rate of cooling and duration of heating at maximum temperature. Further experiments are needed to explore a wider range in parameter space to obtain more observational constraints on the process.

The Rietveld plot of one type II sample is given in Fig. 10. The R values, relating the observations to the model, for type IA samples were typically  $R_p = 6.5\%$  for the profile and  $R_{wp} = 8.2\%$  for the weighted profile and for type II samples were  $R_p = 2.2\%$  and  $R_{wp} = 2.8\%$  indicating very acceptable fits. The sample in Fig. 8(a) had olivine with weight percentage of 56.6% with the remainder being amorphous while the type II sample shown in Fig. 10 had olivine (86.2 wt-%), magnetite (7.2 wt-%) with the remainder being amorphous. The Bragg  $R_B$  factors for the individual crystalline phases were also very acceptable with values less than 4%. Refining the site occupancy factors for the two magnesium and iron sites allowed the calculation of stoichiometry of the olivine as  $Mg_{1.92}Fe_{0.08}SiO_4$ , (i.e. almost pure forsterite) for the type IA sample (Fig. 8(a)) and  $Mg_{1.72}Fe_{0.28}SiO_4$  for the type II sample (Fig. 10). The higher iron content of the type II olivine reflects the greater amount of iron in the starting mixture.

## 6. CONCLUSION

The experiment demonstrates that GRBs can melt precursor dust balls to form chondrules in nearby planetary forming systems in agreement with predictions. Once formed, the chondrules can move through the gas more freely and coagulate to form the building blocks of planets (Cuzzi et al. 2001). GRBs with durations greater than 2 s are associated with supernovae in massive stars and the formation of Kerr black holes (Popham et al. 1999; McBreen et al. 2002b). The discovery of more than 100 extra-solar giant planets has opened a range of

questions regarding the mechanisms of planetary formation (Santos et al. 2003; Laughlin 2000). The probability that any planetary forming system will be blasted by a nearby GRB has been estimated (McBreen & Hanlon 1999; Scalo & Wheeler 2002) to be about 0.1%. In the solar neighbourhood, 7% of stars with high metallicity harbour a planet whereas less than 1% of stars with solar metallicity seem to have a planet (Santos et al. 2003). The GRB method seems to be only one of the mechanisms involved because of the high percentage of stars with planets. There is a further difficulty for the model in the case of our solar system because most chondrules were melted more than once requiring a repeating process (Rubin 2000; Wasson & Rubin 2003). However the formation of planetary systems may be enhanced by the presence of a nearby GRB which will form chondrules across the whole nebula at essentially the same time (McBreen & Hanlon 1999) but would require a range of assumptions about the location of the dust in the disk to account for the properties of chondrules in different classes of chondrites. Advances in the methods of detecting remnant GRBs and planetary systems may reveal a link between them in our galaxy.

A GRB can reveal planetary forming systems in other galaxies because there will be short duration ( $\sim 1$  hour) bursts of infrared radiation from the melted dust when chondrules form across the whole nebula. These infrared bursts can occur for up to several hundred years after the GRB when the expanding shell of radiation melts the dust in planetary forming systems that happen in its way. However the GRB should be in a nearby galaxy to detect the faint infrared bursts with powerful telescopes such as the overwhelmingly large telescope (OWL) and the James Webb Space Telescope (JWST).

## ACKNOWLEDGMENTS

The University College Dublin groups thank Enterprise Ireland for support. We thank Åke Kvik, Gavin Vaughan and Ann Terry for their help in using the ID11 beamline at ESRF. Sheila McBreen and Elaine Winston thank IRCSET for support.

## REFERENCES

- Akerlof, C., Balsano, R., Barthelmy, S., et al. 1999, *Nature*, 398, 400
- Anders, E. & Grevesse, N. 1989, *Geochim. Cosmochim. Acta*, 53, 197
- Band, D., Matteson, J., Ford, L., et al. 1993, *ApJ*, 413, 281
- Boss, A. P. 1996, in *Chondrules and the Protoplanetary Disk*, ed. R. H. Hewins, R. H. Jones, & E. R. D. Scott (Cambridge University Press, Cambridge), p257
- Brearley, A. J. & Jones, R. H. 1998, *Rev. Mineralogy*, 36, 398
- Cameron, A. G. W. 1995, *Meteoritics*, 30, 133
- Ciesla, F. J. & Hood, L. L. 2002, *Icarus*, 158, 281
- Clark, D. H., McCrea, W. H., & Stephenson, F. R. 1977, *Nature*, 265, 318
- Connolly, H. C., Jones, B. D., & Hewins, R. H. 1998, *Geochim. Cosmochim. Acta*, 62, 2725
- Costa, E., Frontera, F., Heise, J., et al. 1997, *Nature*, 387, 783
- Cuzzi, J. N., Hogan, R. C., Paque, J. M., & Dobrovolskis, A. R. 2001, *ApJ*, 546, 496
- Duggan, P., McBreen, B., Carr, A. J., et al. 2003, *A&A*, 409, L9
- Duggan, P., McBreen, B., Hanlon, L., et al. 2001, in *Gamma-ray Bursts in the Afterglow Era*, ed. E. Costa, J. Hjorth, & F. Frontera (Springer Verlag), p294
- Fishman, G. J. & Meegan, C. A. 1995, *ARA&A*, 33, 415
- Grossman, J. N., Rubin, A. E., Nagahara, H., & King, E. A. 1988, in *Meteorites and the Early Solar System*, p619
- Hewins, R., Jones, R., & Scott, E., eds. 1996, *Chondrules and the Protoplanetary Disk* (Cambridge University Press)
- Hewins, R. H. & Fox, G. E. 2004, *Geochim. Cosmochim. Acta*, 68, 917
- Hill, R. J. & Howard, C. J. 1987, *J. Appl. Crystallogr*, 20, 467
- Hunter, B. 1998, *International Union of Crystallography Commission on Powder Diffraction Newsletter*, 22, 21
- Hurley, K., Sari, R., & Djorgovski, S. G. 2002, *astro-ph/0211620*
- Jones, R. H., Lee, T., Connolly, H. C., Love, S. G., & Shang, H. 2000, *Protostars and Planets IV*, 927
- King, E. A., ed. 1983, *Chondrules and their origins* (Lunar and Planetary Institute, Houston, Texas)
- Laughlin, G. 2000, *ApJ*, 545, 1064
- Lee, T., Shu, F. H., Shang, H., Glassgold, A. E., & Rehm, K. E. 1998, *ApJ*, 506, 898
- Lofgren, G. & Lanier, A. B. 1990, *Geochim. Cosmochim. Acta*, 54, 3537
- Mészáros, P. 2002, *ARA&A*, 40, 137
- Maharaj, S. V. & Hewins, R. H. 1994, *Geochim. Cosmochim. Acta*, 58, 1335
- Martin, P. M. & Hughes, D. W. 1980, *Earth and Planetary Science Letters*, 49, 175
- McBreen, B. & Hanlon, L. 1999, *A&A*, 351, 759
- McBreen, S., McBreen, B., Hanlon, L., & Quilligan, F. 2002a, *A&A*, 393, L29
- . 2002b, *A&A*, 393, L15
- McBreen, S., Quilligan, F., McBreen, B., Hanlon, L., & Watson, D. 2001, *A&A*, 380, L31
- McSween, H. Y. 1977, *Geochim. Cosmochim. Acta*, 41, 477
- Miura, H. & Nakamoto, T. 2004, in *Lunar and Planetary Institute Conference Abstracts*, p1612
- Nicastro, L., Amati, L., Antonelli, L. A., et al. 1998, *A&A*, 338, L17
- Piran, T. 1999, *Phys. Rep.*, 314, 575
- Piro, L. 2004, *astro-ph/0402638*
- Popham, R., Woosley, S. E., & Fryer, C. 1999, *ApJ*, 518, 356
- Quilligan, F., McBreen, B., Hanlon, L., et al. 2002, *A&A*, 385, 377
- Remington, B. A., Arnett, D., Drake, R. P., & Takabe, H. 1999, *Science*, 284, 1488
- Rubin, A. E. 2000, *Earth-Science Reviews*, 50, 3
- Rubin, A. E. & Keil, K. 1984, *Meteoritics*, 19, 135
- Ruderman, M. A. 1974, *Science*, 184, 1079
- Santos, N. C., Israelian, G., Mayor, M., Rebolo, R., & Udry, S. 2003, *A&A*, 398, 363
- Scalo, J. & Wheeler, J. C. 2002, *ApJ*, 566, 723
- Scott, H. G. 1981, *Acta. Cryst.*, A37, 456
- Sekiya, M. 1998, *Icarus*, 133, 298
- Sorby, H. C. 1877, *Nature*, 15, 495
- Strohmayer, T. E., Fenimore, E. E., Murakami, T., & Yoshida, A. 1998, *ApJ*, 500, 873
- Swindle, T., Davis, A., Hohenberg, C., et al. 1996, in *Chondrules and the Protoplanetary Disk*, ed. R. H. Hewins, R. H. Jones, & E. R. D. Scott (Cambridge University Press, Cambridge), p77
- Thorsett, S. E. 1995, *ApJ*, 444, L53
- Veigele, N. J. 1973, *Atomic Data Tables*, 5, 51
- Wasson, J. T. 1993, *Meteoritics*, 28, 14
- Wasson, J. T. & Rubin, A. E. 2003, *Geochim. Cosmochim. Acta*, 67, 2239
- Weidenschilling, S. J. & Ruzmaikina, T. V. 1994, *ApJ*, 430, 713
- Wood, J. A. 1988, *Ann. Rev. Earth Planet Sci.*, 16, 53
- Yu, Y. & Hewins, R. H. 1998, *Geochim. Cosmochim. Acta*, 62, 159
- Zhang, B. & Meszaros, P. 2003, *astro-ph/0311321*
- Zinner, E. 1996, *Science*, 271, 41